Evidence for Klein Tunneling in Graphene *p-n* Junctions

N. Stander, B. Huard, and D. Goldhaber-Gordon*

Department of Physics, Stanford University, Stanford, California 94305, USA

(Received 13 June 2008; published 16 January 2009)

Transport through potential barriers in graphene is investigated using a set of metallic gates capacitively coupled to graphene to modulate the potential landscape. When a gate-induced potential step is steep enough, disorder becomes less important and the resistance across the step is in quantitative agreement with predictions of Klein tunneling of Dirac fermions up to a small correction. We also perform magnetoresistance measurements at low magnetic fields and compare them to recent predictions.

DOI: 10.1103/PhysRevLett.102.026807 PACS numbers: 73.23.−b, 73.43.Fj, 73.63.−b

Graphene is promising for novel applications and fundamental physics due to its remarkable electronic, optical, and mechanical properties [1]. At energies relevant to electrical transport, quasiparticles are believed to behave like Dirac fermions with a constant velocity $v_F \simeq 1.1 \times 10^6\ \mathrm{m \cdot s^{-1}}$ characterizing their dispersion relation $E = \hbar v_F k$. The Klein paradox for massless Dirac fermions predicts that carriers in graphene hitting a potential step at normal incidence transmit with probability one regardless of the height and width of the step [2]. At non-normal incidence, this tunneling problem for 2D massless fermions can be represented as a 1D problem for massive Dirac fermions, with the effective mass proportional to the conserved transverse momentum. The Klein tunneling probability should then depend on the profile of the potential step [2–4]. Recent experiments have investigated transport across potential steps imposed by a set of electrostatic gates [5–10], and results of Ref. [9] support an interpretation of Klein tunneling. We present measurements on six devices which allow a quantitative comparison with Klein tunneling in graphene when the potential profile created by the gates is evaluated realistically [11]. Disorder is sufficiently strong in all our devices to mask effects of multiple reflections between the two steps of a potential barrier, so that all data can be accounted for by considering two independent steps adding Ohmically in series. Finally, we probe the transition from clean to disordered transport across a single potential step, and we refine the accuracy of the transition parameter introduced by Fogler *et al.* [12]. In a complementary measurement, we show that the effect of a low magnetic field on the Klein tunneling across a potential step in graphene is not explained by existing predictions in the clean limit [13].

We measure six top-gated graphene devices (typical schematic shown in Fig. 1), whose essential parameters are listed in Table I. The density n_{bg} far from the top-gated region is set by the back gate according to $n_{\mathrm{bg}} = \frac{C_{\mathrm{bg}}(V_{\mathrm{bg}} - V^0_{\mathrm{bg}})}{e}$, where $C_{\mathrm{bg}} = 13.6\ \mathrm{nF \cdot cm^{-2}}$ is the back gate capacitance per area (from Hall effect measurements on a similar wafer oxidized in the same furnace run), e is the electron charge, and V^0_{bg} is the gate voltage required to attain zero average density [14]. The density n_{tg} well inside the top-gated region is set by both back gate and top gate voltages according to $n_{\mathrm{tg}} = n_{\mathrm{bg}} + \frac{C_{\mathrm{tg}}(V_{\mathrm{tg}} - V^0_{\mathrm{tg}})}{e}$, where C_{tg} and V^0_{tg} are the top gate counterparts of C_{bg} and V^0_{bg}. Throughout this Letter we use the notation $\Delta n_{\mathrm{tg}} = n_{\mathrm{tg}} - n_{\mathrm{bg}}$ to identify the contribution of the top gate voltage only, which tunes the potential step height. As described in previous work [5], an asymmetry with respect to $n_{\mathrm{tg}} = 0$ appears in the four-probe resistance measured across a top-gated region as a function of V_{tg} for fixed back gate voltages V_{bg} [Fig. 2(b)]. This asymmetry quantifies the resistance across the potential step in graphene created by the gates. All graphene top-gated devices were fabricated in the same way, which is described in detail in the supporting material [15]. For electrical characterization, samples are immersed in liquid helium at 4 K and four-terminal measurements are made using a lock-in amplifier at a frequency 32 Hz with a bias current of 100 nA. All samples show typical monolayer graphene spectra measured by Raman spectroscopy and exhibit the quantum Hall plateaus characteristic of graphene when measured in perpendicular magnetic fields up to 8 T at 4 K (see supporting material [15]).

In order to extract the resistance of the *p-n* interfaces only, we measure the odd part of resistance R_{odd} about $n_{\mathrm{tg}} = 0$ [5]:

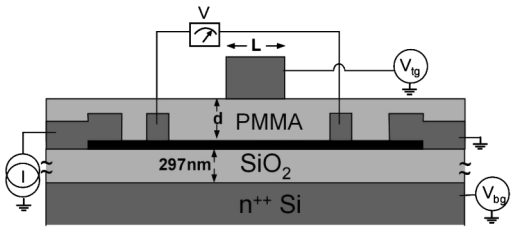

FIG. 1. Schematic diagram of a top-gated graphene device with a four-probe measurement setup. Graphene sheet is black, metal contacts and gates are dark gray.

TABLE I. Geometrical properties of the samples: top gate length L, graphene strip width (interface length) w, and top gate dielectric thickness d. Same letter for two device labels indicates same graphene sheet. All dimensions were taken by both scanning electron microscopy and atomic force microscopy. The transition parameter β between clean and diffusive transport in a single p-n junction is also shown (see text), averaged across the whole measured voltage range such that $n_{bg} < 0$ and $n_{tg} > 0$. Counterintuitively, despite devices' low mobility, $\beta \gg 1$ so that Klein tunneling is expected rather than diffusion across the interface.

Sample	L (nm)	w (μm)	d (nm)	$\langle\beta\rangle$	μ (cm^2 V^{-1} s^{-1})
A60	60	4.3	34	7.6	1800
B100	100	2.1	42	3.8	1700
B220	220	2.1	42	3.5	1700
C540	540	1.74	25	7.9	1400
A860	860	3.6	34	7.9	1800
C1700	1700	1.74	47	1.9	1300

$$2R_{odd}(n_{bg}, n_{tg}) \equiv R(n_{bg}, n_{tg}) - R(n_{bg}, -n_{tg}), \quad (1)$$

where R is the four-probe resistance as a function of the densities far from the top-gated region and well inside that region. Extracting the odd part R_{odd} from the measured resistance requires an accurate determination of the densities n_{bg} and n_{tg}. This is made by the measurement of three independent quantities V^0_{bg}, V^0_{tg}, and C_{tg}/C_{bg}. We carefully measure these quantities by using the quantum Hall measurements at 8 T and electron-hole symmetry [15]. There are two physical interpretations for R_{odd} depending on the relative magnitude of two length scales: the mean free path $l_e = \frac{h}{e^2}\frac{\sigma}{2\sqrt{\pi n}}$ (well defined for $k_F l_e \gg 1$ or equivalently for a conductivity $\sigma \gg 2e^2/h$) and the top gate length L. For $L \gg l_e$, after crossing the first interface of the barrier carriers lose all momentum information before impinging on the second interface. In this case, the total barrier resistance can be modeled by two junctions in series. The expression $2(R_{pn} - R_{pp})$ where R_{pn} (R_{pp}) denotes the theoretical value of the resistance of a single p-n (p-p) interface, can then be compared directly to the experimental quantity $2R_{odd}$ [5]. For $L \ll l_e$, multiple reflections occur between the two interfaces of the barrier, which is predicted to reduce the total barrier resistance [15]. As all devices have modest mobility, we start by using a diffusive model to calculate R_{pn} and R_{pp}. In this model, due to disorder the resistance depends on the local resistivity $\rho(n)$ (measured for a uniform density at $V_{tg} = V^0_{tg}$) at each position x:

$$R^{(dif)}_{pn} - R^{(dif)}_{pp} = \frac{1}{w}\int \rho(n(n_{bg}, n_{tg}, x)) - \rho(n(n_{bg}, -n_{tg}, x))dx. \quad (2)$$

Figure 3 compares the experimental curves for $2R_{odd}$ as a function of V_{tg} at several V_{bg} for samples A60 and C540 to the corresponding predictions. Clearly, the diffusive model represented by the dashed lines predicts resistance values considerably below the experimental curves, hinting that transport through the device cannot be viewed as entirely diffusive. Following the calculation by Fogler *et al.* [12], we retain the diffusive model for the region away from the interface, but replace it by a ballistic interface model for a region extending one mean free path in either direction from the location where density changes polarity [16]. Thus,

$$R_{pn} - R_{pp} = R^{(bal)}_{pn} - R^{(bal)}_{pp} + R^{(dif)}_{pn}|_{x\geq|l_e|} - R^{(dif)}_{pp}|_{x\geq|l_e|}, \quad (3)$$

where the two last terms are taken from Eq. (2), but with the integral excluding $x \in [-l_e, l_e]$. The first two terms are the ballistic contributions to the interface resistance for bipolar and monopolar configurations, and can be calculated individually as follows. All conduction channels on the low-density side of a monopolar junction should have transmission nearly 1 through the junction [17], so $R^{(bal)}_{pp} = \frac{4e^2}{h}\frac{w\sqrt{\pi}\min(|n_{bg}|,|n_{tg}|)}{2\pi}$. The bipolar case was addressed by Zhang and Fogler [11]:

$$R^{(bal)}_{pn} = c_1 \frac{h}{e^2 w}\alpha^{-1/6}|n'|^{-1/3}, \quad (4)$$

where h is Planck's constant, $\alpha = \frac{e^2}{\epsilon_r \hbar v_F} \sim 0.56$ is the di-

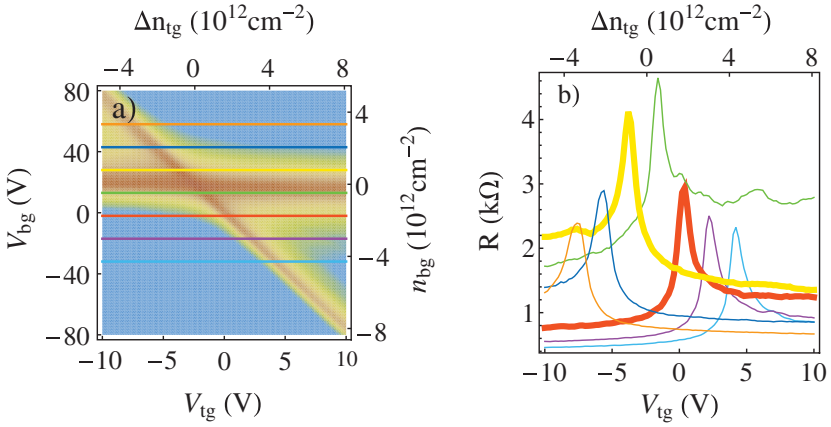

FIG. 2 (color). (a) Four-probe resistance measured on device C540 (see Table I), as a function of V_{bg} and V_{tg}. The color scale can be inferred from the cuts shown in (b). The densities n_{bg} and Δn_{tg} are estimated using $V^0_{tg} = 2.42$ V, $V^0_{bg} = 18.65$ V, and $C_{tg} = 107$ nF $\cdot$ cm^{-2}. (b) Resistance as a function of V_{tg} at several values of V_{bg}. The two bold curves show a clear asymmetry with respect to the peak ($n_{tg} = 0$) for both $V_{bg} < V^0_{bg}$ (red) and $V_{bg} > V^0_{bg}$ (yellow).

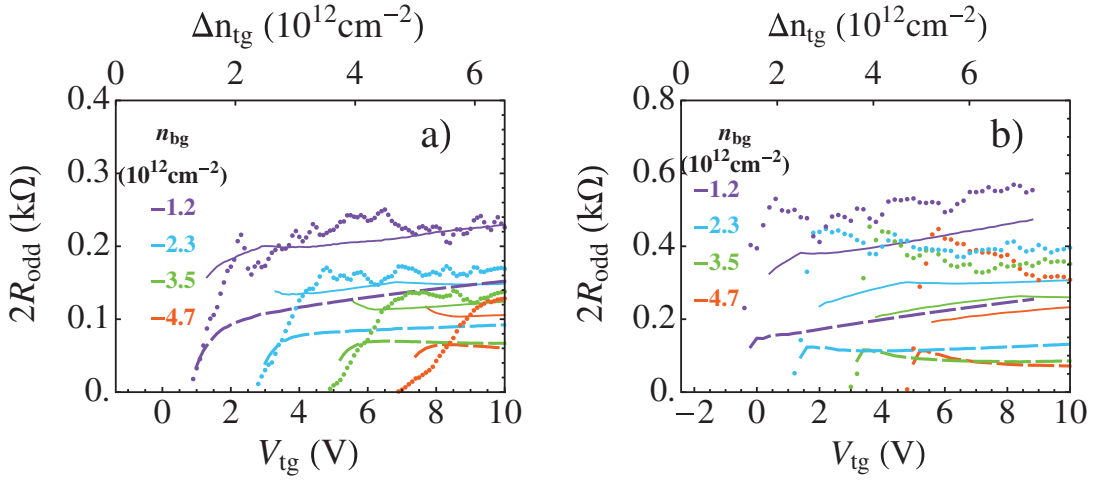

FIG. 3 (color). (a) The series resistance $2R_{\text{odd}}$ of the barrier interfaces as a function of V_{tg}, for several values of V_{bg} for device A60 (corresponding densities n_{bg} are labeled). The measured resistance $2R_{\text{odd}}$ (dots) is compared to the predicted value $2(R_{\text{pn}} - R_{\text{pp}})$ using either a diffusive model, Eq. (2) (dashed lines), or a ballistic model, Eq. (3), with the value $c_1 = 1.35$ chosen to best fit all six devices (solid lines). (b) Same as (a) for device C540.

mensionless strength of Coulomb interactions ($\epsilon_r \approx 3.9$ is the average dielectric constant of SiO_2 and cross-linked polymethyl methacrylate (PMMA) measured at 4 K), and n' is the slope of the density profile at the position where the density crosses zero (density profile calculated from the classical Poisson equation with realistic gate geometry, temporarily treating graphene as a perfect conductor). Expression (4) refines this calculation to take into account nonlinear screening of graphene close to zero density, going beyond the linear model used in Ref. [3]. The prefactor c_1 in Eq. (4) is determined numerically [11]. In our case, $\alpha = 0.56$ and the prefactor is predicted to be $c_1 = 1.10 \pm 0.03$ [18]. In order to test this prediction c_1 will be used as a single fit parameter across all samples and densities. The solid lines in Fig. 3 were generated by Eq. (3), choosing $c_1 = 1.35$ to best account for all experimental curves in all devices (voltages $V_{\text{bg}} > V_{\text{bg}}^0$ give a similar agreement, not shown for clarity). The slight discrepancy between theoretical and experimental values of c_1 might be due in part to exchange and correlation effects. Trying to fit the data using a naive linear potential model requires an independent fitting parameter for each device, and even with the best fit to the data, some qualitative trends of the experimental data cannot be accounted for by this model, as described in detail in the supporting material [15]. This mismatch between the linear model and the data indicates the importance of accounting for nonlinear screening close to zero average density. We continue by calculating the ratio $\eta = R_{\text{odd}}/(R_{\text{pn}} - R_{\text{pp}})$, for all devices, for all measured V_{bg} and V_{tg}, using Eq. (3). The histogram of η is sharply peaked at a certain value η_{peak} with a small peak width [15]. For all devices except C1700, regardless of their length L, η is close or slightly higher than 1 when using $c_1 = 1.35$ (Fig. 4), which indicates that the resistances of both interfaces of the potential barrier simply add in series, and a single p-n junction is less sensitive to disorder than transport between the two interfaces of a potential barrier. Fogler *et al.* introduced the parameter $\beta = n' n_i^{-3/2}$ to describe the clean or disordered transition in a single p-n junction, where n_i is related to the mobility by $n_i = \frac{e}{\mu h}$ [12]. According to Ref. [12], when $\beta \gg 1$ the ballistic contribution in Eq. (3) dominates and the junction is in the clean limit, whereas for $\beta \ll 1$, the diffusive contribution in Eq. (3) dominates and the junction is in the disordered limit. The threshold $\beta = 1$ marks the transition where ballistic contribution must be taken into account since it is comparable to the diffusive contribution. In the following, we refine this transition threshold experimentally. From Fig. 4 and Table I, it seems that transport is indeed well described by Eq. (3) when $\beta > 3.5$ but more poorly for C1700 where $\beta \lesssim 2$, where we find that η is further than 1 and has a large spread of values. In addition, Fogler *et al.* predict that the diffusive contribution to the interface resistance will be negligible for $\beta > 10$, which is reached

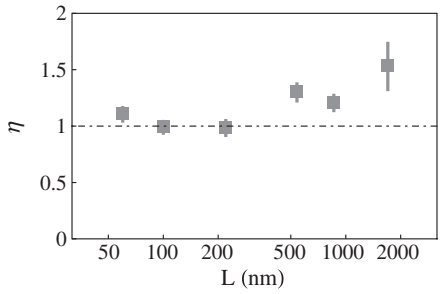

FIG. 4. Symbols: Ratio $\eta = R_{\text{odd}}/(R_{\text{pn}} - R_{\text{pp}})$ as a function of top gate length L for the devices of Table I. R_{pn} is calculated with $c_1 = 1.35$. The vertical lines show the width of the histogram of η for densities such that $|n_{\text{bg}}|, |n_{\text{tg}}| > 10^{12}$ cm^{-2}. The dashed line at $\eta = 1$ corresponds to perfect agreement between theory and experiment, in the case where the total resistance is the sum of the resistances of two p-n interfaces in series.

in several of our devices for densities $n_{tg} > 3 \times 10^{12}$ cm^{-2}. At these densities, in spite of our devices' modest mobility, the junction can be considered as disorder-free since the calculated ballistic contribution to R_{odd} is 10 times higher than the diffusive one, which allows us to make a rather accurate measurement of the ballistic contribution alone in this clean limit, and match it well with the ballistic terms in Eq. (3). In a recent experiment where suspended top gates were used, for one sample the agreement with Eq. (2)—the disordered limit—was very good (sample *S*3 in Ref. [9]). This is due to a much larger distance between the top gate and the graphene sheet, and much smaller density range than in this work, likely due to lower dielectric constant combined with mechanical instability of the top gate when applying higher voltages. These two factors considerably reduce n' (around 80 times), which is not fully balanced by the cleaner graphene of Ref. [9] (n_i 2–5 times smaller). We estimate $\langle \beta \rangle \approx 0.7$ for device *S*3 reported in Ref. [9]. Note that two other devices on substantially cleaner graphene (*S*1 and *S*2 in Ref. [9]) support an interpretation of Klein tunneling with $\beta = 2.5$ and $\beta = 4$, respectively. From this work and from the result of Ref. [9], one can see that the transition between clean and disordered transport in *p*-*n* junctions seems to be sharp: for $\beta > 2.5$ the clean limit applies, for $\beta < 0.7$ the disordered limit applies, and in between neither limit is valid [19].

Being sharply dependent on angle of incidence, transport through potential steps in graphene should be sensitive to the presence of a magnetic field, which bends electron trajectories. For $n_{bg} = -n_{tg}$ the predicted interface conductance in the clean limit is

$$G_{pn}(B) = G_{pn}(0)(1 - (B/B_\star)^2)^{3/4}, \quad (5)$$

where $G_{pn}(0)$ is the conductance at zero field, $B_\star = \hbar(el)^{-1}\sqrt{\pi \Delta n_{tg}}$, and l is the distance over which the potential rises, which is proportional to the thickness d of the oxide [13]. We measure R_{odd}^{-1} as a function of magnetic field B in two devices C540 and C1700 on the same graphene sheet but with different top gate dielectric thickness d (Table I). We use the experimental $G_{pn}(0)$ and the best parameter l to fit all curves within the same device (see supporting material). The parameters l for C540 and C1700 are found to be 65 and 55 nm, respectively, whereas C1700 has the thicker dielectric (see Table I). Further theoretical work is needed to explain this discrepancy.

In conclusion, we show evidence for Klein tunneling across potential steps in graphene with a quantitative agreement to a model with one free parameter describing screening properties in graphene. The crossover between clean and disordered regimes occurs as a function of the parameter β around 1 as predicted by Fogler *et al.* [12]. More work is needed to go into the fully ballistic regime, and also to measure directly the angle dependence of Klein tunneling [3].

We thank J. A. Sulpizio for help with fabrication and characterization, and M. Fogler, D. Novikov, L. Levitov, and A. Young for enlightening discussions. We also thank A. Savchenko for pointing out the need to take into account the resistance of the monopolar junction in the predictions for R_{odd}. This work was supported by the MARCO/FENA program and the Office of Naval Research Contract No. N00014-02-1-0986. N. S. was supported by a William R. and Sara Hart Kimball Stanford Graduate Grant. Work was performed in part at the Stanford Nanofabrication Facility of NNIN supported by the National Science Foundation under Grant No. ECS-9731293. Critical equipment (SEM, AFM) was obtained partly on Air Force Grants No. FA9550-04-1-0384 and No. F49620-03-1-0256.

Note added.—While this work was under review, we became aware of related work by Young *et al.*, in which evidence is seen for ballistic transport across a full *n*-*p*-*n* junction [20].

*Corresponding author.
goldhaber-gordon@stanford.edu

[1] A. H. Castro Neto *et al.*, Rev. Mod. Phys. (to be published).
[2] M. I. Katsnelson, K. S. Novoselov, and A. K. Geim, Nature Phys. **2**, 620 (2006).
[3] V. V. Cheianov and V. I. Fal'ko, Phys. Rev. B **74**, 041403 (2006).
[4] C. Beenakker, Rev. Mod. Phys. **80**, 1337 (2008).
[5] B. Huard *et al.*, Phys. Rev. Lett. **98**, 236803 (2007).
[6] J. R. Williams, L. DiCarlo, and C. M. Marcus, Science **317**, 638 (2007).
[7] B. Özyilmaz *et al.*, Phys. Rev. Lett. **99**, 166804 (2007).
[8] Jeroen B. Oostinga *et al.*, Nature Mater. **7**, 151 (2008).
[9] R. V. Gorbachev *et al.*, Nano Lett. **8**, 1995 (2008).
[10] Gang Liu, Jairo Valesco, Jr., Wenzhong Bao, and Chun Ning Lau, Appl. Phys. Lett. **92**, 203103 (2008).
[11] L. M. Zhang and M. M. Fogler, Phys. Rev. Lett. **100**, 116804 (2008).
[12] M. M. Fogler *et al.*, Phys. Rev. B **77**, 075420 (2008).
[13] A. V. Shytov, Nan Gu, and L. S. Levitov, arXiv:0708.3081.
[14] J. H. Chen *et al.*, Nature Phys. **4**, 377 (2008).
[15] See EPAPS Document No. E-PRLTAO-102-016904 for additional material about characterization, fabrication, analysis, and experimental results. For more information on EPAPS, see http://www.aip.org/pubservs/epaps.html.
[16] The mean free path is a function of carrier density, and hence it varies as one approaches the interface. Following Fogler *et al.* [12] we self-consistently define a distance x_{bal} over which transport near the interface is ballistic: $l_e[n(x_{bal})] = x_{bal}$, where the interface is at $x = 0$, $n(x)$ is derived from solution of the classical Laplace equation for the actual device geometry, and $l_e = \frac{\hbar}{2e}\mu\sqrt{n(x)/\pi}$.
[17] J. Cayssol *et al.*, arXiv:0810.4568.
[18] M. M. Fogler (private communication).
[19] Near $n_{tg} \approx 0$, where density fluctuations are bigger than n_{tg}, disorder should dominate [12].
[20] A. Young *et al.*, Nature Phys. (to be published).